Romanian Journal of Mechanics
Volume 2, Issue 1/2017, pp 37-50, ISSN 2537 - 5229, rjm.journals.srmta.ro

ON THE TRANSIENT FLOW OF BLOOD IN ARTERIES

Veturia CHIROIU [*] , Valeria MOSNEGUTU [*] , Andrei C. VASILESCU [**] , Antonio GLIOZZI [***]

[*] Institute of Solid Mechanics, Romanian Academy
[**] Technical University of Civil Engineering Bucharest, Romania
[***] Politecnico di Torino, DISAT -Dipartimento Scienza Applicata e Tecnologia, Italy

Corresponding author: Veturia CHIROIU, E-mail: veturiachiroiu@yahoo.com

Abstract In this work we analyze the transient blood flow in the arterial system, subjected to arbitrary arterial pressure consisting of two solitons, with application to the thoracic aorta of the dog. The artery is modelled as a highly flexible infinite elastic tube with thin, straight, circular and homogeneous walls embedded in the tissue. It is assumed that blood is an incompressible micropolar fluid. The flow rate, micro-gyration and cross-sectional area are calculated as functions of blood pressure pulse. The effects of increasing of the hematocrit on the magnitude of flow velocity and micro-gyration are analyzed. Seven micropolar viscosity coefficients are introduced as function of the initial particle concentration and are reconstructed by a genetic algorithm based on experimental data.

Key words: Transient flow, blood vessels, micropolar fluid, Fahraesus-Lindquist effect.

1. INTRODUCTION

The blood is a complex fluid being a suspension of particles (red and white cells, platelets) undergoing unsteady flow through vessels. Blood flow in arteries is dominated by unsteady flow phenomena. The arteries can adapt and change with the varying hemodynamic conditions. The most literature on this topic concentrates on a microscopic view, more precisely on the micropolar fluids, firstly introduced by Eringen [1]. This theory exhibits micro-rotational effects such as those experienced by blood in the larger vessels of the circulation for the dog [2].

Ariman, Turk and Sylvester [3] have applied in 1974 the Eringen theory for describing the time-dependent blood flow. Their model formulates a new kinematic variable called microrotation describing the individual rotation of particles within the continuum, independent of the velocity field. In this theory, an arbitrary pressure gradient as a sum of and was considered to describe the pulsatile character of the flow. But the pulsatile character of the blood flow suggests and using the soliton theory.

The pressure pulse contains an increase and a decrease in amplitude in accordance with the increase and decrease of the pulse velocity. Yomosa [4] proposed in 1987 a soliton theory for modelling the motion of blood.

Equations describing a nonlinear model of blood flow were first written by Euler in 1775 [4]. In 1956 Lambert has suggested firstly to use the method of characteristics for computations of the blood flow problems. Using the numerical integration, the method of characteristics, the finite difference method or other numerical approaches important investigators have solved interesting problems concerning the blood flow into arteries for the linear or nonlinear cases. For more details see [2 -12].

Blood is a complex mixture of cells, proteins, lipoproteins, and ions by which nutrients and wastes are transported. Red blood cells typically comprise approximately 40% of blood by volume. Because red blood cells are small semisolid particles, they increase the viscosity of blood and affect the behavior of the fluid. Blood is approximately four times more viscous than water.

The nonlinear theories that have been developed are all one dimensional. The thin-walled elastic tube is infinitely long, straight, circular and homogeneous embedded in the tissue and filled with the blood. The blood motion in vessels with small radius is analyzed in [6] for a micropolar fluid containing deformable material particles with six degrees of freedom: three translations, three rotations and six stretch and shears.

In the present work, the features of arterial blood flow are interpreted in the viewpoint of a two-soliton solution. Our model is extending the Yomosa model [4], by considering an arbitrary two-soliton blood pressure field for a micro-continuum model of blood.

The basic governing equations consist of two equations of micropolar fluid motion, the equation of continuity and the Yomosa relationship between the cross-sectional area and the pressure of blood appropriate to a nonlinear elastic model of the tube wall. Seven micromolar viscosity coefficients are introduced as a function of the initial particle concentration and are reconstructed by a genetic algorithm based on experimental data.

The cnoidal method is applied to solve the set of nonlinear dynamic equations of the blood motion. By using the theta-function representation of the solutions and a genetic algorithm, the ventricular motion is describable as a linear superposition of cnoidal pulses and additional terms, which include nonlinear interactions among them [13-16].

2. THEORY

In this paper, we consider the one-dimensional fields of longitudinal flow-velocity $v(x,t)$, the micro-gyration $w(x,t)$, the blood pressure $p(x,t)$ and the cross- sectional area $A(x,t)$ under the assumption of uniform distributions of v and p over the cross-section of the tube. Here x is the axial distance along the vessel and t, the time. The radial component of the flow-velocity is neglected in comparison with the axial component. The dimensional governing equations of the micropolar fluid dynamics are given by [16-19]

$$v_{,t} + vv_{,x} + \rho^{-1}(p_{,x} - (\alpha+\mu)v_{,xx} - \alpha w_x) = 0, \tag{1}$$

$$jw_{,t} + \rho^{-1}(\alpha v_{,x} - \gamma w_{,xx} + 2\alpha w) = 0, \tag{2}$$

$$A_{,t} + (vA)_{,x} = 0, \tag{3}$$

where ρ is the fluid density, α, μ, γ the blood coefficients and j the micro-inertia coefficient $j = 2\gamma/(2\mu+\alpha)$. The coefficient α depends on the cellular concentration (hematocrit) and is determined from the equation [13]

$$\alpha^2 + \alpha(2\mu - \gamma q^2) - \gamma q^2 \mu = 0 \ , \tag{4}$$

where q has been found experimentally $q = 10^5\,\mathrm{m}^{-1}$ [13], μ represents the viscosity of blood plasma (0.002 Pa·s at $30^0 C$ [3]). The ratio $1/q$ is defining the red cell diameter for blood. To obtain the relationship between A and p we consider the motion equation of the wall given by Yomosa

$$\rho_0 h r_{,tt} - (p - p_e) = h\sigma r^{-1}, \tag{5}$$

with ρ_0 the density of the material of the wall, $r(x,t)$ the radius of the tube, h the thickness of the wall in radial direction, p_e the pressure outside the tube which can be regarded as about the same as the atmospheric pressure, σ the extending stress in the tangential direction.
The density of the materials of the wall and the tissue are assumed to be equal. Noting by h_0 the equilibrium values of the thickness of the wall and the by r_0 the equilibrium radius of the tube for $p = p_e$ the condition for the conservation of mass of the wall is given by $rh = r_0 h_0$.

Defining

$$r = r_0 + u \ , \ \sigma = Eur_0^{-1}(1 + \alpha u r_0^{-1}), \tag{6}$$

where u is the radial displacement of the wall, E the Young's modulus of the elasticity, a a non-linear coefficient of elasticity, (5) becomes

$$\rho u_{,tt} = (p - p_\varepsilon)h^{-1} - Eu(r_0 + au)/r_0^2(r_0 + u), \tag{7}$$

Substituting in (7) $A = \pi(r_0 + u)^2$ we obtain the motion equation of the cross-sectional area

$$A_{,tt} - 0.5A^{-1}A_{,t}^2 - \rho_0^{-1} f(A, p) = 0, \tag{8}$$

$$f(A, p) = 2\sqrt{\pi A}h^{-1}(p - p_\varepsilon) + 2(2a - 1)\sqrt{\pi A}Er_0^{-1} - 2Ear_0^{-2}A + 2E\pi(1 - a). \tag{9}$$

Dimensionless equations of motion can be written as

$$v_{,t} + vv_{,x} + p_{,x} - mv_{,xx} - nw_{,x} = 0, \tag{10}$$

$$bw_t + qv_{,x} - gw_{xx} + dw = 0, \tag{11}$$

$$A_{,t} + (vA)_{,x} = 0, \tag{12}$$

$$A_{,tt} - 0.5A^{-1}A_{,t}^2 - f(A, p) = 0, \tag{13}$$

$$f(A, p) = b_1 p\sqrt{A} + b_2\sqrt{A} - b_3 A + b_4. \tag{14}$$

where

$$\begin{gathered} m = (\alpha + \mu)\xi, \ \ n = \alpha c^0 \xi \ \ , \ \ b = jl_0^{-2}, \ \ q = \alpha\xi, \\ g = \gamma t_0 \zeta, \ \ d = \alpha t_0 l_0^2 \zeta, \ \ \xi = 1/\rho c_0^2 t_0, \\ \zeta = (\rho l_0^4)^{-1}, \ \ b_1 = 2\rho c_0^2 h^{-1} E^{-1}, \ \ b_2 = 2r_0^{-1}(2a - 1), \\ b_3 = 2ar_0^{-1}, \ \ b_4 = 2r_0^{-1}(1 - a). \end{gathered} \tag{15}$$

These equations are derived by introducing the change of variables

$$\begin{gathered} l_0 = \sqrt{r_0 h_0 \rho_0 / 2\rho}, \ \ t_0 = \sqrt{r_0 \rho_0 / E}, \ \ c_0 = l_0 t_0^{-1}, \ \ x' = xl_0^{-1}, \\ t' = tt_0^{-1}, \ \ v' = vc_0^{-1}, \ \ p' = (p - p_\varepsilon)/\rho c_0^2, \ \ w' = t_0 w, \ \ A' = AA_0^{-1}, \ \ A = \pi r^2, \ \ r' = rr_0^{-1}. \end{gathered} \tag{16}$$

in (17)-(21) . Let us assume an unsteady arbitrary pressure gradient of the form

$$p(x,t) = \sum_{i=1}^{2} A_i \operatorname{sech}^2(\hat{b}_i - kx + \omega t), \tag{17}$$

with A_i , $\hat{b}_i$, k unknown constants and ω the circular frequency.

The governing equations (12)-(17) are solved by using the cnoidal method [9]. The initial conditions are

$$\begin{aligned} v(0,0) &= v_0\,, \quad v_{,t}(0,0) = v_1\,, \\ w(0,0) &= w_0\,, \quad w_{,t}(0,0) = w_1\,, \\ A(0,0) &= a_0\,, \quad A_{,t}(0,0) = a_1\,. \end{aligned} \tag{18}$$

3. SOLUTIONS

The solutions $x = (v, w, A)$ of (10)-(18) are expressed as the sum between a linear superposition

$$x_{lin}(\tau) = \int_{-\infty}^{\infty} \alpha \mathrm{cn}^2[\tilde{\omega}t; \tilde{m}]\mathrm{d}\tau\,, \tag{19}$$

and a nonlinear superposition of cnoidal vibrations

$$x_{int}(\tau) = \int_{-\infty}^{\infty} \frac{\tilde{\beta}\mathrm{cn}^2[\tilde{\omega}t; \tilde{m}]}{1+\tilde{\lambda}\mathrm{cn}^2[\tilde{\omega}t; \tilde{m}]}\mathrm{d}\tau\,. \tag{20}$$

where $\tilde{\omega}_j$ are the frequencies and $0 \le \tilde{m} \le 1$.

In the general case, the flow of blood solutions of the problem can be expressed as

$$x_j(t) = \int_{-\infty}^{\infty} K_j(t) g(t-\tau)\mathrm{d}\tau = \int_{-\infty}^{\infty} K_j(t-\tau) g(\tau)\mathrm{d}\tau, \quad j = 1,2,3, \tag{21}$$

where

$$K_j(t) = \exp(-\nu t)\sum_{k=1}^{n}\left[\mathrm{cn}^2[\tilde{\omega}_{jk}t; \tilde{m}_{jk}] + \frac{\tilde{\beta}_{jk}\mathrm{cn}^2(\tilde{\omega}_{jk}t, \tilde{m}_{jk})}{1+\tilde{\gamma}_{jk}\mathrm{cn}^2(\tilde{\omega}_{jk}t, \tilde{m}_{jk})}\right].$$

The solution requires the evaluation of unknowns $\tilde{\omega}, \tilde{m}, \tilde{\beta}$ and $\tilde{\gamma}$. Substitution of (21) and (22) into (10)-(18) gives a set of identities from which the parameters are evaluated. The identities results by equating the coefficients for expression terms containing the functions cn and sn in the same power.

The solutions are calculated from

$$x_j(t) = \int_{-N}^{N} K_j(t) g(t-\tau)\mathrm{d}\tau, \quad j = 1,2,3, \tag{22}$$

where the choice of N depends of the required accuracy, which in our cases is 7 digits. We have considered $N = 10$ for the constant excitation frequency problem, and $N = 15$, for the time-dependent excitation frequency problem, respectively. The functions $K_j(t)$, $j = 1,2,3$, are calculated from

$$K_j(t) = 2\pi\sum_{k=1}^{n}\frac{1}{\tilde{K}_{jk}\sqrt{m_{jk}}}\sum_{p=0}^{P} Z_{jkp}^2(t) + 2\pi\sum_{k=1}^{n}\frac{\dfrac{\tilde{\beta}_{jk}}{\tilde{K}_{jk}\sqrt{m_{jk}}}\displaystyle\sum_{p=0}^{P} Z_{jkp}^2(t)}{1+\tilde{\gamma}_{jk}\dfrac{2\pi}{\tilde{K}_{jk}\sqrt{m_{jk}}}\displaystyle\sum_{p=0}^{P} Z_{jkp}^2(t)},$$

with

$$Z_{jkp}(t) = \frac{q_{jk}^{p+1/2}}{1+q_{jk}^{2p+1}}\cos(2p+1)\frac{\pi\tilde{\omega}_{jk}t}{2\tilde{K}_{jk}}.$$

The profiles of the flow velocity, the blood pressure and the cross-sectional area are calculated using the data obtained from the thoracic aorta of the dog measurements [3, 13]

$$\rho_0 = 1.06\times 10^3 \ \text{Kg/m}^3\ ,\ \rho\ = 1.05\times 10^3 \ \text{Kg/m}^3$$

$$r_0 = 5\times 10^{-3}\ \text{m}\ ,\ \ h_0 = 0.6\times 10^{-3}\ \text{m}\ ,\ \ E = 5.49\times 10^5\ \text{Pa}$$

$$\omega = 23.273\ \text{rad/s}\ ,\ \ p_e = 10897\ \text{Pa}$$

For the blood coefficients, we choose $\mu = \alpha = 0.002\text{Pas}$, $\gamma = 0.6\text{mkg/s}$ and $j = 20\text{m}^2$. By equating the width of the blood pressure two-soliton wave to the width (the wave-length is 162cm) of the pulse wave observed experimentally for thoracic aorta of the dog we obtain $T = 0.27\text{s}$ and $c = 6\text{m/s}$.

The dimensionless form of initial conditions (18) is chosen as

$$\begin{aligned} v(0,0) &= 0.5\,,\quad v_{,t}(0,0) = 0\,,\\ w(0,0) &= 0.3\,,\quad w_{,t}(0,0) = 0\,,\\ A(0,0) &= 1.5\,,\quad A_{,t}(0,0) = 0\,. \end{aligned} \tag{23}$$

Figs. 1 and 2 plot the blood pressure and the micro-gyration for two periods. It is seen that the systolic and diastolic peaks exist in all graphs. The systolic and diastolic pressure peaks are related to the flow velocity peaks.

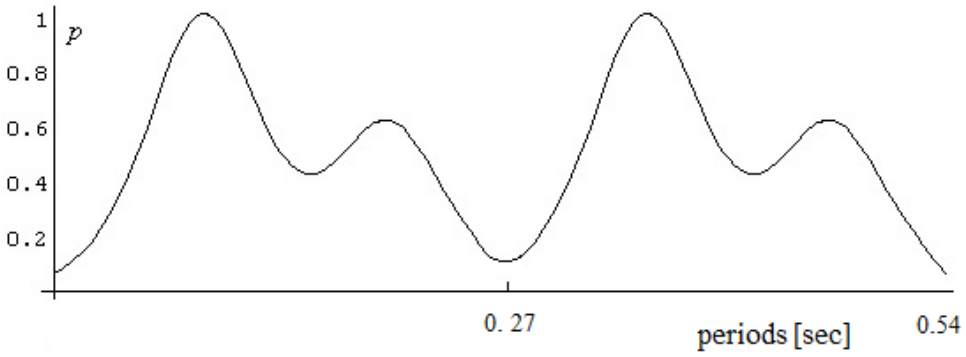

Fig. 1. Variation of the blood pressure in two periods.

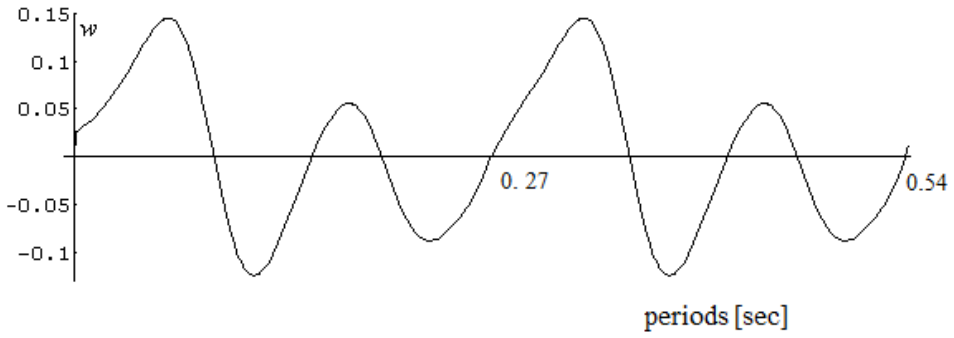

Fig. 2. Variation of the micro-gyration in two periods.

The scenario for variation of coefficient α gives the effect of the volume concentration of the red cell upon the flow behaviour of blood. To illustrate the effect of hematocrit on the flow velocity and on the micro-gyration we consider several values of α.

The phase portraits for flow-velocity and the micro-gyration are plotted in Figs. 3 and 4 after four periods. For an increasing number of periods the graphs remain unchangeable.

The motion becomes stable, the role of the initial conditions being very small.

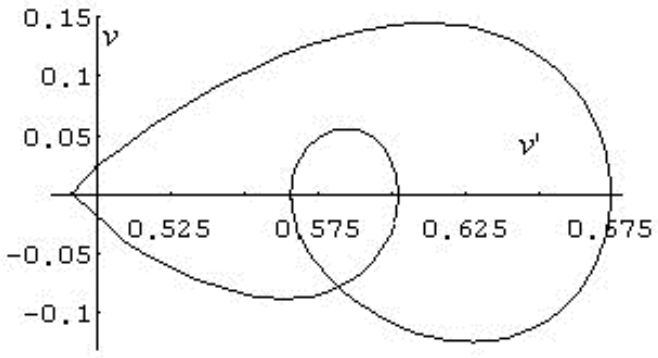

Fig. 3. Phase portrait for the flow velocity after four periods.

The blood viscosity is a reflection of hematocrit. Viscosity increases when red-cell density is high or flow rates are low, and cells are ready to aggregate. Aggregates increase resistance to flow. Turbulent blood flow is less efficient than streamline flow because kinetic energy is dissipated through chaotic motion.

Chaotic attractors usually appear in regions where flow velocities are high such as when blood is forced through narrowing of blood vessels. For example, for narrowing the area by 10%, the attractor (v, v', w) after 10 periods with chaotic tendency is shown in Fig. 5.

In fig. 6 the cross-sectional area is plotted for one period. Figs. 7 - 8 show a decreasing of the amplitude of the flow velocity and of the micro-gyration for increasing hematocrit. The blood flow falls as hematocrit rises.

The results are reasonable due to the fact for increasing hematocrit.

The results are reasonable due to the fact that the increase of viscosity overshadows the inertial effects leading to a reduction of the amplitudes and are in agreement with the experiments [3].

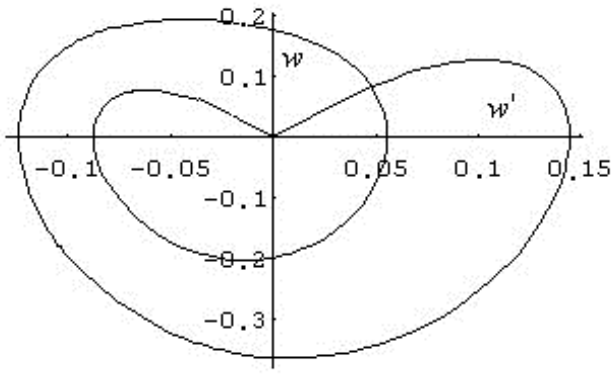

Fig. 4. Phase portrait for micro-gyration after four periods.

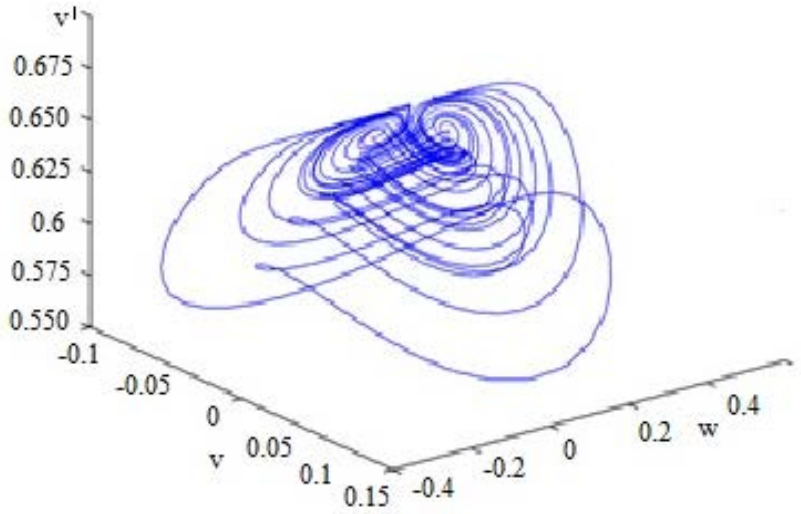

Fig. 5. Atractor (v, v', w) after 10 periods.

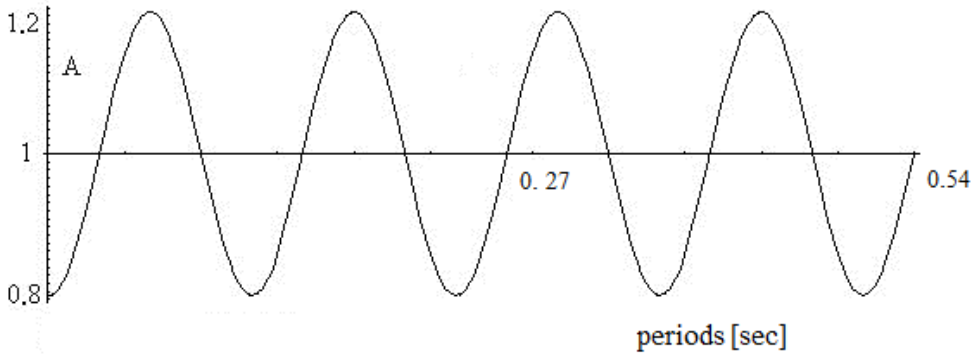

Fig. 6. Variation of area in two periods.

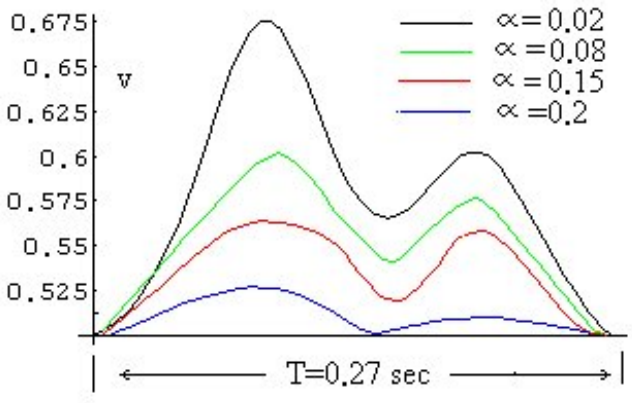

Fig. 7. Effect of the hematocrit on the flow velocity.

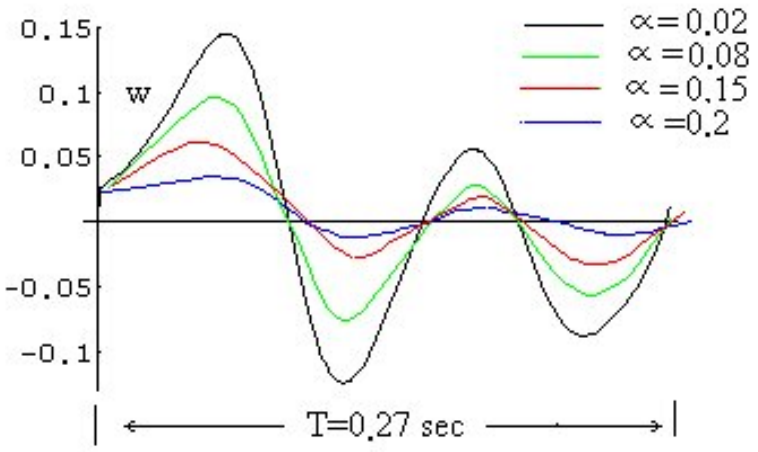

Fig. 8. Effect of hematocrit on the micro-gyration.

4. MICROPOLAR VISCOSITY COEFFICIENTS

In the previous theory, only one viscosity coefficient was considered. The blood modeled as a micropolar fluid is characterized by 7 coefficients of viscosity. It is possible to evaluate these coefficients through an inverse problem using experimental data [20-22].

Let us consider the dissipation function Φ by the form

$$\Phi = -\tilde{p}(x,t)a_{kk} + \Phi_1, \tag{24}$$

where $\tilde{p}$ is a Lagrange multiplier. The functions Φ_1 depends on the invariants of the vector and tensor variables and is given by

$$2\Phi_1 = \mu_v \mathrm{tr}(a^2) + 2(\mu_v + 2\sigma_v + \eta_v)\mathrm{tr}(c^2) + 4(\mu_v + \sigma_v)\mathrm{tr}(ac) + (\mu_v + \kappa_v)\mathrm{tr}(aa^T), \tag{25}$$

where $\mu_v, \sigma_v, \kappa_v$ and η_v are viscosity coefficients for the stress tensor. The restrictions placed on these moduli to make $\Phi \geq 0$ for all independent variations of a_{kk}.

The micropolar viscosity coefficients [6] are functions of the initial particle concentration and now we show that a genetic algorithm based on experimental data can reconstruct them.

The problem to be addressed here is the inverse of the forward problem.

We seek to determine information about the viscosity coefficients by using experimental information concerning the $x = (v, w, A)$ of (10) -(18), for blood flow in circular tubes of different diameters.

The aim is to use the difference between experimental $V_j^{\exp} = \{w(r_j),\ j = 1,2,...m\}$, and predicted by theory velocities $V_j = \{w(r_j),\ j = 1,2,...m\}$ to provide a procedure, which iteratively corrects the controlling parameters towards values leading to the least discord between predictions and experimental observations.

The controlling parameters are the viscosity coefficients $\beta_v = \{\mu_v, \kappa_v, \sigma_v, \eta_v\}$, which are functions of the initial particle concentration c, and piecewise continuous on $c_{\min} \leq c \leq c_{\max}$.

To extract the the viscosity coefficients β_v from the experimental data, an objective function must be chosen to measure the agreement between theoretical and experimental data. This objective function is built on the base on three restrictions expressed as three terms

$$\Im(\beta_v) = m^{-1}\sum_{j=1}^{m}(V_j - V_j^{\exp})^2. \tag{26}$$

The objective function (26) is maximized by using a genetic algorithm for determining an accurate set of unknowns, so that the residuals must have the values very close to zero. These residuals evaluate the verification of all governing equations and boundary conditions and assure the existence and uniqueness of results.

We define fitness as follows

$$F = \frac{\Im_0}{\Im}, \tag{27}$$

with

$$\Im_0 = m^{-1}\sum_{j=1}^{m}(V_j^{\exp})^2 . \tag{28}$$

As the convergence criterion of iterative computations, the expression Z must be maximum

$$Z = \frac{1}{2}\log_{10}\frac{\Im_0}{\Im} \to \max . \tag{29}$$

The quality of the model depends on the maximum value of the function Z. We show that the knowledge of the experimental data $V_j^{\exp} = \{w(r_j),\ j = 1,2,...m\}$ is sufficient to determine the coefficients β_{vi}, $i = 1,2,3,4$.

The numerical experiments show that for $m < 100$, the genetic algorithm has no solution. For m above this value, we obtain one, two or more solutions. In all our examples presented in the next section we considered $m = 171$.

The experimental data $V_j^{\exp} = \{w(r_j),\ j = 1,2,...m\}$, are furnished by [13-17] for tubes of different diameters.

A part of the measurements data is made with a scanning capillary-tube rheometer used for measuring both the viscosity and yield stress of blood without any anticoagulant and other part with a Haake Rotovisco RV100 viscometer.

The results of the genetic algorithm are the values of the viscosity coefficients. Tables 1 and 2 present the viscosity coefficients $[10^{-3}\,\mathrm{Pa}\cdot\mathrm{s}]$ for the $40\,\mu\mathrm{m}$ tube, and respectively for the $199\,\mu\mathrm{m}$ tube.

An important result is related to Fahraesus and Lindquist effect. By applying the inverse approach, it results a decreasing of the viscosity coefficients μ_v for increasing the tube radius from $12\,\mu\mathrm{m}$ to 14.6, and a decreasing of the viscosity coefficients μ_v for decreasing the tube radius from $20\,\mu\mathrm{m}$ to 14.6 results. The results are presented in Figs. 9 and 10. We refer to $R_c = 14.6\,\mu\mathrm{m}$ as the critical radius of μ_v. For $R > R_c$ the viscosity coefficients μ_v is increasing.

The viscosity coefficients depend not only on the initial concentration but also on the tube size. The Fahraesus-Lindquist effect of decreasing of the viscosity effects with a decreasing tube radius is observed. The values for μ_v and κ_v, corresponding to the $199\,\mu\mathrm{m}$ tube, are larger than those of the $40\,\mu\mathrm{m}$ tubes with maximum 0.8–0.9%, and the rest of the constants with maximum 0.2–0.3%, with an exception of σ_v.

But the absolute values of σ_v respect the Fahraesus-Lindquist effect [29]. The predicted values of the table 1 agree with most experimental values [25].

Table 1. The viscosity coefficients [$10^{-3}\,\mathrm{Pa}\cdot\mathrm{s}$] for a tube of 40 μm diameter.

c	μ_v	κ_v	σ_v	η_v
0.9	2.222	0.651	– 4.001	7.306
0.85	2.148	0.610	– 4.592	6.991
0.8	2.023	0.579	– 4.359	6.823
0.75	2.157	0.509	– 3.004	5.055
0.7	1.865	0.411	– 2.431	3.078
0.65	1.621	0.344	– 1.877	2.989
0.6	1.543	0.306	– 1.548	2.679
0.55	1.455	0.281	– 0.464	2.330
0.5	1.263	0.256	– 0.345	1.673
0.45	1.143	0.201	– 0.356	1.757
0.4	1.112	0.185	– 0.330	1.937
0.35	1.014	0.155	– 0.321	1.707
0.3	0.906	0.107	– 0.206	0.613
0.25	0.802	0.077	– 0.133	0.565
0.2	0.711	0.063	– 0.125	0.450
0.15	0.601	0.053	– 0.103	0.358
0.1	0.488	0.046	– 0.101	0.355

Table 2. The viscosity coefficients [$10^{-3}\,\mathrm{Pa}\cdot\mathrm{s}$] for a tube of 199 μm diameter.

c	μ_v	κ_v	σ_v	η_v
0.9	2.345	0.644	– 4.010	6.306
0.85	2.065	0.544	– 3.879	6.432
0.8	2.012	0.456	– 3.774	5.804
0.75	1.973	0.339	– 2.139	5.001
0.7	1.740	0.241	– 1.737	4.079
0.65	1.701	0.201	– 1.480	2.589
0.6	1.609	0.187	– 1.301	2.279
0.55	1.532	0.148	– 0.516	2.032
0.5	1.463	0.142	– 0.428	1.644
0.45	1.341	0.122	– 0.337	1.257
0.4	1.303	0.100	– 0.305	1.037
0.35	1.210	0.069	– 0.233	1.007
0.3	0.829	0.017	– 0.220	0.810
0.25	0.714	0.013	– 0.157	0.666
0.2	0.622	0.009	– 0.123	0.552
0.15	0.600	0.008	– 0.115	0.334
0.1	0.566	0.007	– 0.113	0.311

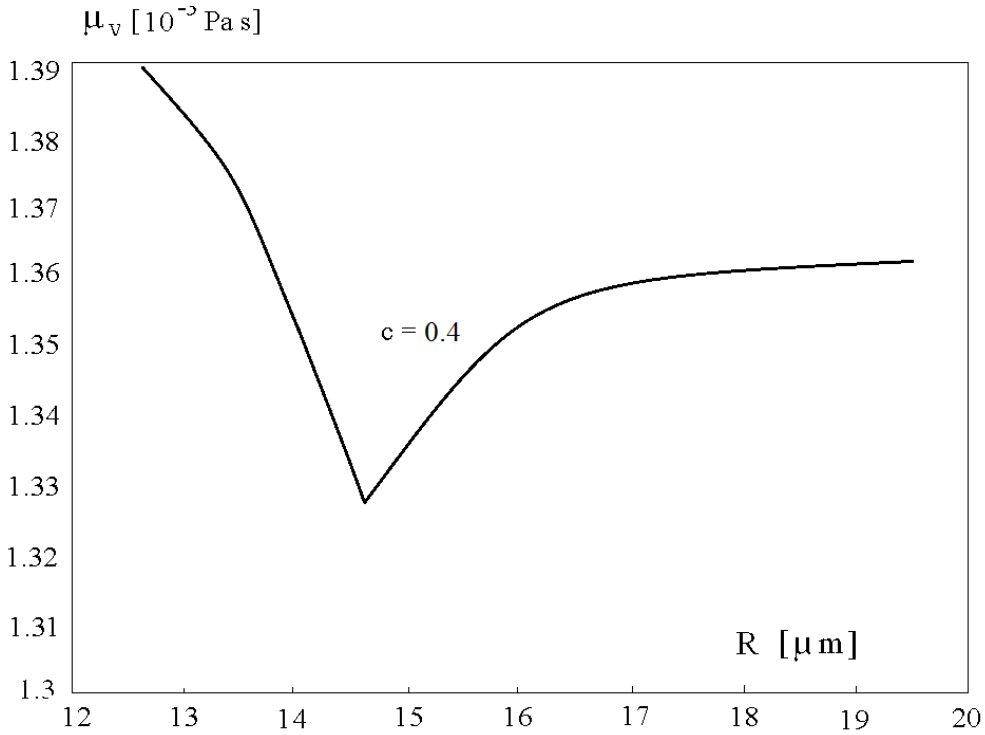

Fig. 9. Variation of the viscosity coefficients μ_v with decreasing tube radius, and c = 0.4.

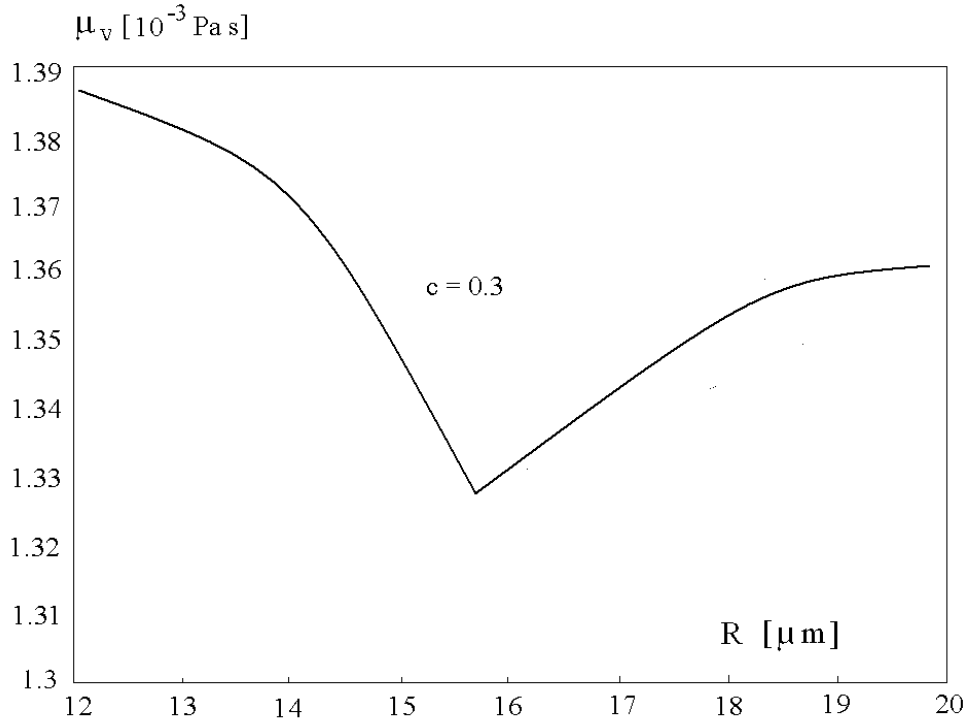

Fig. 10. The variation of the viscosity coefficients μ_v with decreasing tube radius (c = 0.3).

The last result is the study of the dependence of the viscosity coefficient μ_v on the shear rate (s^{-1}), which is shown in Fig. 11, for two tubes of $R = 10.6\,\mu m$, $c = 0.4$, and $R = 9.7\,\mu m$, $c = 0.2$. This is in a good agreement with the observations on some physical phenomena observed in the blood motion through small vessels [8, 26-28, 30, 31].

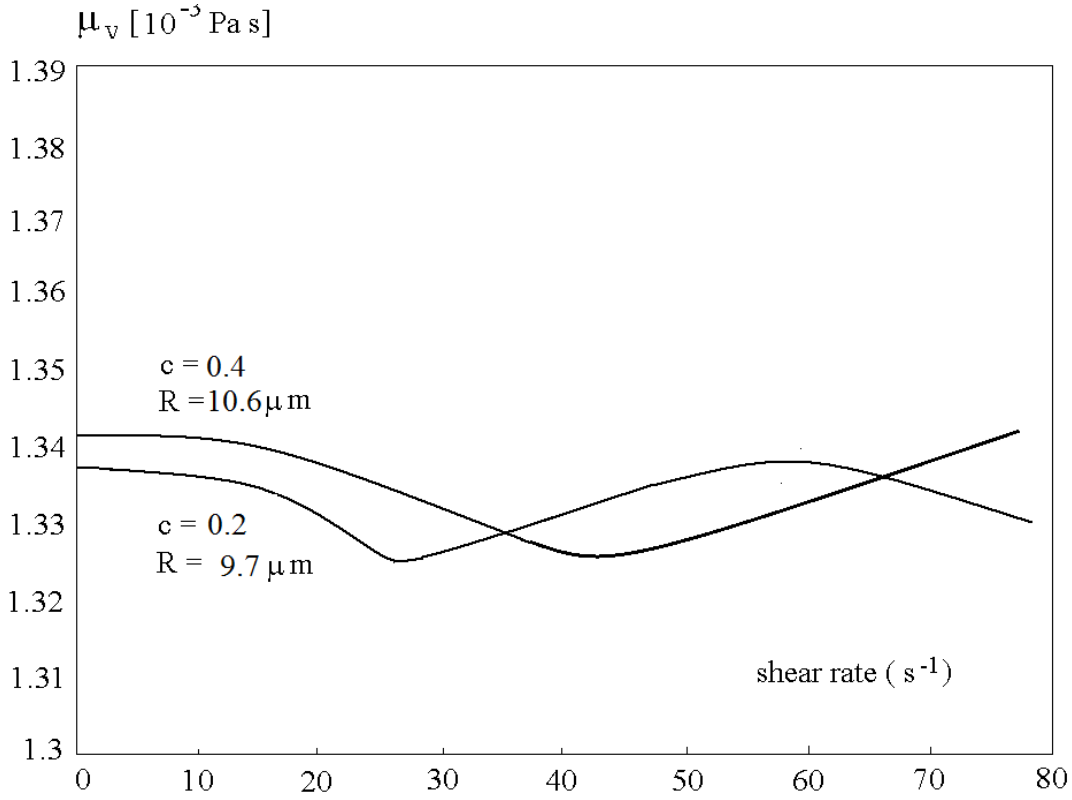

Fig. 11. The variation of the viscosity coefficients μ_v with shear rate.

5. CONCLUSIONS

In this paper, the transient blood flow in large arteries is analysed using a micropolar model of blood. The Newtonian and non-Newtonian fluid models for blood theory fail in explanation of these phenomena, because of the microstructure in the blood.

The motion of red cells, white cells and platelets in the human blood plasma have a specific effect on the motion of blood in small circular vessels, which cannot be explained by the Newtonian and non-Newtonian fluid theories.

The difference between the micropolar theory and the classical theory of blood consists in that couple stresses and internal micromoment of inertia. In the micropolar theory, the motion is described not only by a deformation but also by a microrotation giving six degrees of freedom.

The interaction between the blood components is transmitted not only by a force but also by a torque, resulting in asymmetric force stresses and couple stresses. The blood is modelled as a micropolar fluid containing particles with six degrees of freedom.

The theory is used for reconstruction of the viscosity coefficients from available experimental data, by using a genetic algorithm. The two-soliton representation for the blood pressure may be viewed as an interaction of two pulses. They are superimposed but retain their identity and do not destroy each into the flow. This assures the stability of the blood circulation.

The flow velocity, the micro-gyration and the cross-sectional are calculated as functions of the two-soliton blood pressure pulse. The phase portraits demonstrate the stability of the blood motion.

The theory of micropolar fluids supports the observation of major physical phenomena observed, such as the Fahraesus-Lindquist effect of decreasing of the apparent viscosity with a decreasing tube radius.

Also, we believe that the micropolar theory of the motion of blood in small vessels highlights the understanding of the viscous properties of blood necessary in generation of blood microflow in microelectromechanical systems specialized for blood analysing and medical applications.

REFERENCES

1. ERINGEN, A.C., *Theory of micropolar fluids*, J. Math. Mech., 16, 1-18, 1966.
2. MCDONALD, D.A., *Blood flow in arteries*, Edward Arnold, London, 2nd ed., 1974.
3. ARIMAN, T., TURK, M.A., SYLVESTER, N.D., O*n time-dependent blood flow*, Letters in Appl. and Engn. Sci., 2, 21-36, 1974.
4. YOMOSA, S., *Solitary waves in large blood vessels*, Journal of the Physical Society of Japan, 56(2), 506-520, 1987.
5. MOODIE, T.B., SWATERS, G.E., *Nonlinear waves and shock calculations for hyperelastic fluid-filled tubes*, Quarterly of Applied Mathematics, 47(4), 1989.
6. ARIMAN, T., SYLVESTER, N.D., TURK, M.A., *Microcontinuum fluid mechanics - A review*, Int. J. Eng. Sci., 11, 905, 1973.
8. BARBEC, J.H., COEKLET, G.R., *Prediction of blood flow in tubes with diameters as small as 29 microns*, Microvascular Research, 3, 17–21, 1971.
9. BRULIN, O., *Linear micropolar media*, *in mechanics of micropolar media* (eds. O.Brulin and R.K.T.Hsieh), World Scientific, 87–146, 1982.
10. BUGLIARELLO, G., SEVILLA, J., *Velocity distribution and other characteristics of steady and pulsatile blood flow in fine glass tubes*, Biorheology, 7, 85–107, 1970.
11. CHIEN, S., *Shear dependence of effective cell volume as a determinant of blood viscosity*, Science, 168, 977, 1970
12. CHIROIU, V., CHIROIU, C., BADEA, T. AND RUFFINO, E., *A nonlinear system with essential energy influx: the human cardiovascular system*, 1, 1, 41–45, 2000.
13. MUNTEANU, L., DONESCU, ST., CHIROIU, V., *An inverse problem for the motion of blood in small vessels*, Physiological Measurement, 27, 865-880, 2006.
14. MUNTEANU, L., CHIROIU, C., CHIROIU, V., *Nonlinear dynamics of the left ventricle*, Physiological Measurement, 23, 1-19, 2002.
15. CHIROIU, V., MOSNEGUȚU, V., MUNTEANU, L., IOAN, R., *On a micromorphic model for the synovial fluid in the human knee*, Mechanics Research Communications, 37(2), 246-255, 2010**.**
16. MUNTEANU, L., DONESCU, ST., *Introduction to soliton theory*: *applications to mechanics*, Book series fundamental theories of physics, vol.143, Kluwer Academic Publishers, Dordrecht, Boston (Springer Netherlands) 2004.
17. HASHIZUME, Y., *Nonlinear pressure wave propagation in arteries*, Journal of the Physical Society of Japan, 57(12), 1988.
18. EASWARAN, C.V., MAJUMDAR, R.A., *A uniqueness theorem for incompressible micropolar flows*, Quarterly of Applied Mathematics, 48(2), 1990.
19. WHITHAM, G.B., *Comments on periodic waves and solitons*, IMA Journal of Applied Mathematics, 32, 353-366, 1984.
20. GOODALE, W.T., LUBIN, M., ECKENHOFF, J.E., HAFKENSCHIEL, J.H., BANFIELD W.G., *Coronary sinus catheterization for studying coronary blood flow and myocardial metabolism.* American Journal of Physiology, 152, 340, 1948.
21. GOODALE, W.T., HACKEL, D.B., *Measurement of coronary blood flow in dogs and man from rate of myocardial nitrous oxide desaturation.* Circulation Research, 1, 502, 1953.

22. HACKEL, D.B., GOODALE, W.T., *Effects of hemorrhagic shock on the heart and circulation of intact dogs*, Circulation Resesarch, 1, 628, 1955.
23. CHANSKY, M., LEVY, M.N., *Collateral circulation to myocardial regions supplied by anterior descending and right coronary arteries in the dog*. Circulation Research, 11, 414, 1962.
24. LOVE, W.D., BURCH, G.E., *Differences in the rate of RB8 (uptake by several regions of the myocardium of control dogs and dogs receiving z-norepinephrine or pitressin*, Journal of Clinical Investigation, 36, 479, 1957.
25. SKALAK, R., KELLER, S.A., SECOMB, T.W., *Mechanisms of blood flow*, Journal of Biomechanics Engineering, 103, 102, 1981.
26. KIM, S., *A study of non-newtonian viscosity and yield stress of blood in a scanning capillary-tube rheometer*, PhD Thesis, Drexel Univ., 2002.
27. ERINGEN, A.C., *Microcontinuum Field theories, II Fluent Media*, Springer, 1998.
28. OLIVER III, J..D., *The viscosity of human blood at high hematocrits*, Master of Science thesis, Mass. Inst. of Techn., 1986.
29. FAHRAEUS, R. LINDQUIST, T. *Viscosity of blood in narrow capillary tubes*, American Journal of Physiology, 96, 562, 1931
30. HAYNES, R. H., *The rheology of blood*, Trans. Soc. Rheol., 5, 85–101, 1961.
31. KANG C K., ERINGEN, A.C., *The effect of microstructure on the rheological properties of blood*, Bull. Math. Biol., 38 135–59, 1976.

Received February 22, 2017